Preferred citation: V. Ottesen, E.D. Roede, K. Syverud and Ø.W. Gregersen. Focused ion beam tomography as a means for characterization of CNF in a paper matrix. In **Advances in Pulp and Paper Research, Oxford 2017**, *Trans. of the XVIth Fund. Res. Symp. Oxford, 2017*, (W. Batchelor and D. Söderberg, eds), pp 595–609, FRC, Manchester, 2018. DOI: 10.15376/frc.2017.2.595.

FOCUSED ION BEAM TOMOGRAPHY AS A MEANS FOR CHARACTERIZATION OF CNF IN A PAPER MATRIX

Vegar Ottesen[1], Erik Dobloug Roede[1], Kristin Syverud[1,2] and Øyvind Weiby Gregersen[1]

[1] Norwegian University of Science and Technology (NTNU), Department of Chemical Engineering, Høgskoleringen 1, 7491 Trondheim, Norway
[2] Paper and Fibre Research Institute (PFI), Høgskoleringen

ABSTRACT

A method to study Cellulose Nanofibril (CNF) distribution in three dimensions within a paper matrix – *in-situ* – was developed. Focused Ion Beam (FIB)/Scanning Electron Microscopy (SEM) tomography was used to investigate the distribution of cellulose nanofibers in three dimensions within a paper structure. Sufficient resolution and material contrast was obtained using both secondary and back-scattered electrons in volumes as large as 10^3 μm^3. Challenges and approaches to achieve this are discussed, both with respect to the microscopy technique and with respect to image processing and volume reconstruction. A range of recorded images and reconstructed 3D volumes show the technique capable of resolving CNF in a paper matrix. Results presented show CNF within the paper matrix forming capsules enclosing filler particles. These capsules are seen to only infrequently be in physical contact with the enclosed particles. Similar separation between CNF and enclosed filler particles was tested and confirmed in CNF films with 10 wt% added ground calcium carbonate.

INTRODUCTION

Paper as a material derives its properties from its complex three-dimensional structure. The interplay of paper components within this structure determines the paper's physical and optical properties. For this reason, techniques able to investigate the three-dimensional structure, such as X-ray tomography, have been of interest to paper researchers and manufacturers.

Recent years has seen a strong increase in research and patent focus on cellulose nanofibrils (CNF) as a material [1]. Much of this research, which is covered in several recent review articles [2–6], deal with the addition of CNF to paper furnish for improved mechanical properties. While a range of studies deal with the subject, actual applications of superresolution microscopy techniques with 3D capability to investigate CNF's interactions, distribution within the paper matrix are lacking, and to our knowledge no peer-reviewed literature addressing the question exists at the moment of writing.

One way to attain nanoscopic resolution in three dimensions is sequential imaging and cutting/milling or grinding of the surface, followed by imaging with a sufficiently high-resolution surface technique. By intermittent imaging and cutting, it is possible to reconstruct a tomograph after image acquisition is complete. For optimal results, a technique capable of resolving nanoscopic features and cutting of slices with nanometer thickness and precision is necessary. Nanoscale slicing can be achieved using focused ion beam (FIB) instruments, which can also image the sample using the ion beam [7]. However, current scanning ion beam microscopy (SIM) instruments cannot achieve the imaging resolution of high quality scanning electron microscopy (SEM), and is generally not excellent at contrast when imaging samples with low median atomic number. The novel and versatile FIB-SEM dual-beam systems mediate this by using an ion beam for milling, and a SEM, commonly a field-effect gun (FEG) for imaging. Such dual-beam systems are capable of resolving nanoscopic features using the electron beam, and of cutting nano-scale slices with adequate precision, using the ion beam. While extensively used in biology to investigate subcellular features [8], the technique has, to our knowledge, not previously been used on paper materials.

MATERIALS AND METHODS

Handsheet and film preparation

CNF was prepared from Claflin ground bleached softwood kraft pulp by homogenization. The first homogenization pass was run at 600 bar while subsequent four passes were run at 1 kbar using a Rannie 15 type 12.56x homogenizer. No chemical

pretreatment was used. After production, fibril diameter was measured using transmission electron microscopy (TEM) and atomic force microscopy (AFM), as reported in [9]. In brief, TEM samples were stained with uranyl acetate 1% w/v in water for 60 seconds and drop cast on TEM grids. AFM samples were drop cast on freshly cleaved Mica and examined in tapping mode AFM. To avoid tip-sample convolution, fibril diameter was measured using fibril height, not width. Production and characterization is described in more detail elsewhere [9, 10].

Handsheets containing CNF examined in the current paper were prepared as described by [10]. Samples selected for FIB/SEM inspection contained 30 wt% ground calcium carbonate (GCC) and 5 wt% CNF. In short, samples imaged in the current paper were prepared by mixing TMP, CNF and GCC, stir the resulting furnish for two minutes prior to retention aid addition and handsheet formation. A two component retention aid system consisting of Kemira Fennopol 3500P and Kemira Altonit SF was used. A conventional handsheet former with closed water circulation was used. Further details are as described in [10].

In addition to handsheets, 20 g/m^2 films of 90/10 wt% CNF/GCC were prepared by gravity assisted dewatering. 10 wt% GCC was added to a CNF suspension and stirred vigorously prior to film formation.

Preparation of handsheets for FIB/SEM

Approximately 25 mm^2 samples were cut from selected handsheets. These samples were negatively stained with uranyl acetate (UA). Staining was performed by submersion in a 1% UA solution (in ethanol) for 20 minutes followed by washing with ethanol. Stained samples were embedded in an EpoFix™ two-part epoxy resin. Air bubbles were removed by vacuum treatment prior to hardening in room temperature over night. A cross-section through the sample was made with a scalpel, exposing the embedded sample. A Hitachi IM 4000 ion beam was used to further remove approximately 100 μm from the revealed cross-section, removing artefacts from the scalpel cut and polishing the revealed surface. The IM 4000 instrument uses an Ar^+ ion beam and was used on the samples for 6 hours using 3.8 kV acceleration voltage. After ion milling, the samples were mounted for FIB/SEM inspection and sputter-coated with 20 nm Pt/Pd coating.

FIB/SEM processing

Images for reconstruction were recorded using a FEI Helios Nanolab dual-beam FIB/SEM, and the FEI Slice and View G2 software was used to automate the image acquisition. A volume of interest (VOI) was located by back-scattered electron (BSE) examination of the surface using 15 keV acceleration voltage. BSE images were recorded in low voltage SEM (LV-SEM) mode using 2 keV

acceleration voltage to avoid charging and reduce interaction volume. 1.4 nA beam current and 30 μs dwell time was used with an Everhart-Thornley (ET)-detector set to detect backscattered electrons. For secondary electron (SE) an acceleration voltage of 2 keV and current of 1.4 nA were used. Milling of sections was performed using 93 pA (shown BSE micrographs) or 280 pA (shown SE micrographs) ion beam current, as indicated in relevant captions. Images depicting artefacts were recorded using 3 keV acceleration voltage and 0.69 nA beam current after an ion milling using 6 nA. Images have been recorded using both BSEs and SEs. CNF/GCC films were not examined with FIB/SEM as the dual-beam capability was not necessary to record the desired micrographs.

CNF/GCC film SEM analysis

Cross-sections of films composed of CNF with 10 wt% GCC were prepared by ion beam milling using 3.8 kV for 12 hours. After milling the cross-section was sputter-coated with 12 nm gold and imaged in a Hitachi SU3500 SEM using 5 kV acceleration voltage and a solid-state annular BSE-detector. Seven images aligned along the produced cross-section were recorded with 40% overlap. The images were stitched together using Grid/Collection stitching in FIJI.

Image processing

Micrographs were post-processed using FIJI [11]. Post processing of FIB/SEM micrographs involves aligning of images using the scale-invariant feature transform (SIFT) algorithm [12]. The images were merged into a TIFF-stack, and brightness and contrast were adjusted according to the stack histogram. Gaussian noise on BSE micrographs was reduced by application of a median filter using a 3 × 3-pixel large neighborhood. Given uneven background illumination a pseudo-flat field background removal was performed. The flat-field was constructed from a mosaic composed of the epoxy background from the recorded images and blurred using Gaussian blur with a radius of 50 pixels. Background removal for SE-images is discussed later. Contrast between materials, z-contrast, was used in thresholding to produce two binarized stacks. Stack one contained pixels brighter than the background and stack two contained pixels identified as GCC. A dilation step was performed on stack two, and the result was subtracted from stack one to produce a stack containing pixels identified as cellulose. During binarization the images were corrected for FIB/tilt by elongating each image's y-axis by $1/\sin(52°)$.

Using Matlab Image Processing Toolbox the contact area between cellulose and GCC was estimated. By comparing the GCC and cellulose binary image stacks with one another, pixel by pixel in three dimensions, a new binary image stack may be produced, showing areas where cellulose and GCC are in contact.

Contact was defined as pixels where one of these binary stacks transitions from positive to negative along either *x, y* or *z*-direction while the other stack makes the opposite transition. Results from in- and out-of plane examinations were combined to one image stack. From the image stack depicting contact area a numerical value was determined by counting pixels with positive values.

After post processing, thresholded images were stitched together to 3D reconstructions using Amira software from Visage Imaging and FEI.

Background removal and segmentation of SE-micrographs

Image alignment and brightness/contrast adjustments were performed as for BSE micrographs before further processing. Background removal for micrographs recorded using SE was attempted using pseudo-flat field correction of image brightness.

Several techniques were used to produce the background for this subtraction. FIJI's built-in sliding paraboloid/rolling ball correction was employed [13]. Three different applications of regression as a means of background removal were also attempted. A script was written for "R" producing background estimates from first or second order two-dimensional regression [14]. The basis for these regression models was brightness values from arbitrarily selected points on electron micrograph background. These were manually selected from blurred versions of the images to be processed. A gaussian blur with a radius of 4 pixels was used. The resulting models were used to produce a gradient, which was later subtracted from the unblurred stack. Similar approaches from plugins written for ImageJ were also used, specifically "Nonuniform Background Removal" [15], which uses regions of interest for data gathering as opposed to single points. The last regression implementation used was a plugin titled "A-Posteriori Shading Correction", which divides the processed images by generated gradients [16]. These were applied without the initial gaussian blur.

For further processing, "Nonuniform Background Removal" [15] was used. While the plugin does work on stacks of multiple images generation of a single gradient and division of the entire image stack by this gradient produced a preferrable result. Division was performed using FIJI's Image Calculator Plus, and multiplied by a factor of 55 for increased brightness. From the background corrected stack, one image was extracted and used to create a classifier using the Weka trainable segmentation tool [17]. Training was performed using the sobel, hessian, neighbor and structure training features enabled.

RESULTS AND DISCUSSION

The use of FIB/SEM tomography on insulating samples such as paper can yield high resolution 3D reconstructions of the paper samples, but paper – an

insulating material composed of materials with low median atomic weight – is challenging to image at high resolution without a conductive coating and without topographical contrast.

Sample preparation and image retrieval

To record volumetric information from a non-conductive, composite material such as paper, the sample needs to be carefully prepared and attention given to the microscope's settings. Retrieved images must be possible to binarize with information from only one plane in the reconstructed 3D structure. This means each imaged surface must be as flat as possible, without voids. Embedding in, for example, epoxy, prior to FIB tomography solves this issue by filling in the voids. Though epoxy, like wood fibers, CNF and GCC, is non-conductive – and as a conductive coating cannot be applied to the imaged surfaces sample charging may occur in FIB/SEM tomography (Figure 1).

Sample charging can introduce a range of artefacts in an insulating sample, such as paper embedded in a non-conductive epoxy matrix. To reduce the charge buildup in the insulating sample, it is beneficial to operate the SEM at or near the E_2 equivalency point to avoid buildup of either positive ($E_1 < E_0 < E_2$) or negative ($E_0 < E_1 | E_0 > E_2$) charge. These equivalency points, where E_0 is the acceleration voltage, E_2 and E_1 are energy levels where the electron yield $\delta(E_0) = 1$, and unity is achieved. For most solids, E_2 is in the range of 0.5–3 keV [18]. The E_2 equivalency point depends on a range of factors, including both electron beam incidence angle and sample composition [18–20]. Given its dependence on sample composition, the precise E_2 at a given incidence angle will vary locally in a composite such as paper. Local variations in E_2 can result in charging artefacts appearing in portions of the micrograph (Figure 1 a). In our current work, operating at an an acceleration voltage of 2–3 keV has been seen to work well, depending on the signal source, SE or BSE (Figure 1).

Reducing the acceleration voltage below approximately 5 kV has certain benefits and challenges beyond the effect on charging. Most apparent is the reduced electron penetration depth, leading to a potentially higher resolution for BSE imaging, especially for lighter elements [18, 21]. Furthermore, SE-yield is increased and charging artefacts more easily avoided. However, as the acceleration voltage is reduced, so is the material contrast, and surface topography becomes increasingly dominant as a source of contrast for both SE and BSE signals [19, 20].

Imaging at 2–3 keV, with a current of 1.3 nA and a sample tilt of 52° (Figure 2), is shown to avoid charging while retaining sufficient material contrast to separate cellulose, epoxy and GCC in BSE. Furthermore, at this acceleration voltage, $E_0 \approx E_2$, hence SE yield ($\delta(E_0) \approx 1$), and SE signal carries sufficient material

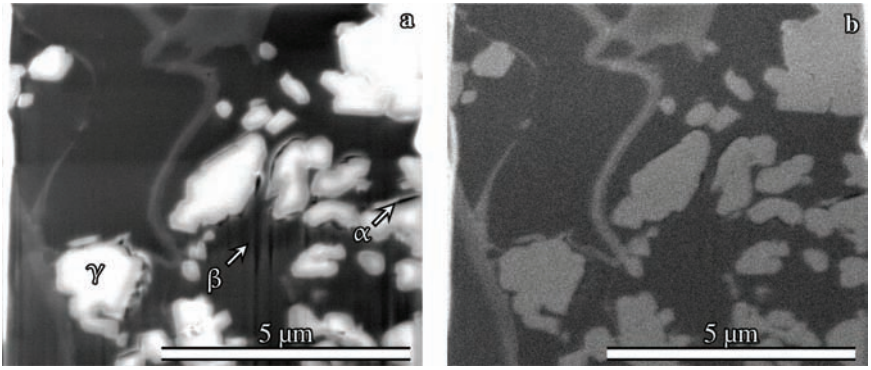

Figure 1. Difference between SE and BSE. Unlevelled electron-micrographs of paper microstructure recorded after milling of trenches. Light gray to white areas are GCC particles. Cellulose shows up somewhat darker, whereas the epoxy is the darkest shade of gray in the images. (a) shows secondary electrons, (b) shows backscattered electrons. Arrows in (a) indicate cracks in the epoxy surrounding GCC particles (α) or curtaining (β). Curtaining is visible as vertical stripes. Negative charge is revealed as bright areas in the center of GCC particles (γ). (b) shows characteristic gaussian noise, but topographical contrast from (a) is less notable. 3 kV acceleration voltage and 0.69 nA beam current used for both micrographs.

contrast to retrieve compositional information using SE as well as BSE [19, 20]. Using SE as a signal source opens for further reduction of the volume contributing to image formation, increasing surface detail and reducing bleed through from features buried underneath the imaged surface [19–21]. It is worth noting, however, that cellulose and epoxy are less dissimilar in SE-micrographs, making computer assisted segmentation more challenging. An additional complicating factor is SEs higher degree of topographical contrast as compared to BSE at used (or higher) acceleration voltages (Figure 1). As such, the smoothness of the imaged surface is paramount if SE is to be used. Several steps can be used to ensure a nanoscopically smooth surface during tomography acquisition, thereby reducing the likelihood of FIB-induced artefacts. A smooth metallic coating on the sample surface can obscure surface topography and compositional changes, both of which can lead to uneven milling rates and subsequent artefacts. Besides a metallic coating, using a low ion beam current during the milling of each slice will reduce beam diameter, further reducing likelihood of artefact formation [22, 23].

As the surface to be imaged is in the *x*–*y*-plane (Figure 2), normal to the sample surface, free escape trajectories for electrons become a concern. To increase the likelihood of escaping electrons being picked up by the detector, as opposed to being trapped by the sample geometry, trenches were milled around the VOI (Figure 2).

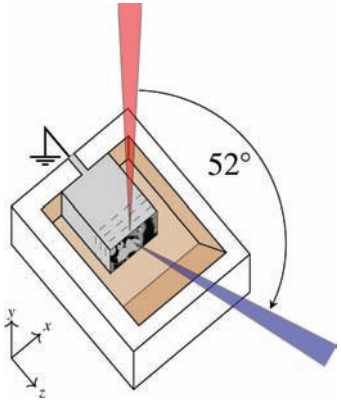

Figure 2. Sample preparation and imaging in FIB/SEM. After location of a VOI, a trench (brown) is milled around the VOI using the ion beam (red). 500 nm platinum (gray) is thereafter applied to the top and sides of the VOI using ion-beam induced deposition (IBID). A 500 nm thick conductive wire of platinum to ground (outside the displayed figure) is also deposited. Tomography of the VOI is performed by imaging the exposed side with the electron beam (blue). After each image, the ion beam is used to mill a thin slice off the VOI as indicated by the dashed lines on the figure, exposing a polished side for imaging. The figure is not to scale. The denoted angle between electron and ion beam (52°) is instrument specific to the FEI Helios Nanolab dual-beam FIB/SEM system.

While the use of low acceleration voltages and currents reduces charge, further steps are necessary to reduce charge buildup and associated effects such as drift. A means of removing electrons from the imaged area is necessary. While the sample preparation does involve application of a conductive coating prior to use of the FIB/SEM instrument, this is insufficient for several reasons. For one, the coating does not extend into the sample volume and is therefore less efficient at removing electrons from portions of the VOI far from the sample surface. Secondly the coating must be thick enough to protect the VOI from damage sustained by repeated SIM during the tomography run; the ion beam is used to image the area of interest. 20 nm PtPd will offer some protection from infrequent SIM during initial alignment prior to preparation of the VOI. Such a coating also permits BSE at higher voltages to reveal underlying composition, facilitating location of VOI. However, the 20 nm PtPd coating does not offer sufficient protection against the repeated SIM use during the experiment proper; the tomography software automatically records SIM-images to align the ion beam prior to each slice. Recording of such SIM micrographs cause damage to the sample area, eventually removing the 20 nm coating initially applied. To ensure the sample remains protected from ion beam damage and that electricity continues to be

conducted away from the imaged area, IBID is used to deposit 500 nm Pt to the top and the sides of the VOI as well as to a point outside the area to be imaged by SIM, thereby grounding the VOI, removing electrons from it. These measures are shown in Figure 2.

Image processing and volume reconstruction

Volumes were recorded using both SE and BSE. Pixel sizes of 13 × 16 nm were achieved using BSE (Figure 3), whereas a resolution of approximately 7 × 9 nm was obtained using SE, at the cost of introduced artefacts and reduced cellulose-epoxy contrast (Figure 1). For volume reconstruction, the third dimension will be 15 nm, the thickness of one slice. The mean fibril diameter was measured to 10.7 nm using AFM and 11.96 nm using AFM.

Backscatter electron micrographs

BSE micrographs have a lower resolution and higher gaussian noise level than SE (Figure 1), but segmentation of these micrographs is possible by simple image processing. As no feature in a micrograph is perfectly sharp, the binarization will lead to a loss of information as the boundaries between objects can often times not be clearly distinguished with pixel-high accuracy. However, quantitative estimates for properties can be obtained, such as contact between cellulose and GCC (Figure 4).

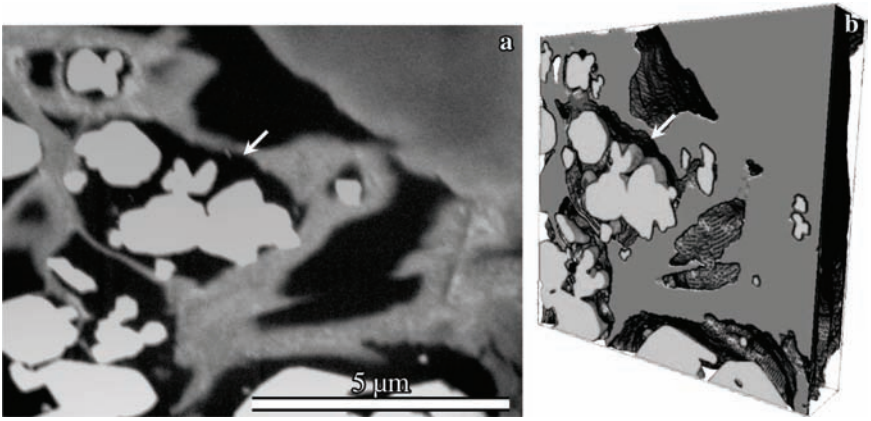

Figure 3. A levelled BSE-micrograph (a) and the 3D reconstruction of which it is a part (b). GCC is shown as bright gray. Cellulose is shown as darker gray. The displayed volume is 12.2 × 9.7 × 1.9 µm large with a voxel size of 13 × 13 × 15 nm. It has been elongated in the *y* direction from (a) to compensate for sample tilt. Pixel size in (a) is 13 × 16 nm. Arrows point to the same point on a cellulose capsule encompassing a small GCC cluster.

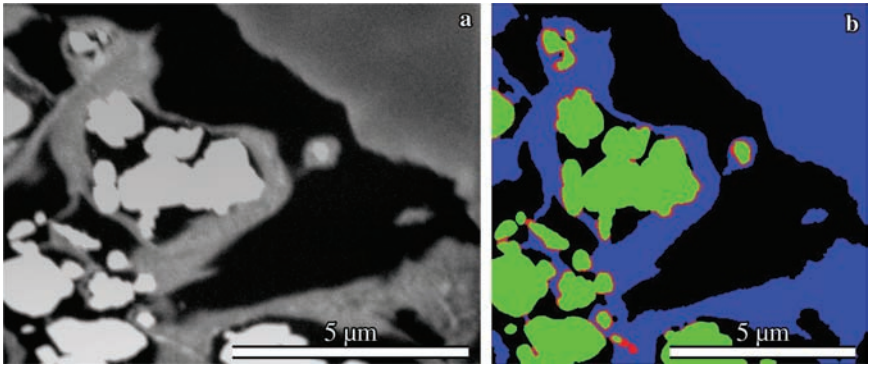

Figure 4. A levelled BSE-micrograph (a) and segmented image with contact area between cellulose and GCC shown in red (b). Contact area has been dilated by 2 pixels for greater visibility. Portion of GCC surface area in contact with cellulose was estimated to 43%.

SE micrographs contain less uniform background (epoxy) brightness and is more prone to topography-induced artefacts making segmentation more challenging. SE signal does reduce Gaussian noise, while simultaneously increasing theoretically achievable resolution. Material contrast is also maintained at the used voltages, the contribution to contrast from structural components means separation of cellulose and epoxy matrix is non-trivial (Figure 5). For recorded volumes the epoxy background is unevenly bright, with local brightness variations due to local micro or nano-topography. It follows that the epoxy and cellulose are difficult to distinguish. Some degree of segmentation was achieved, but the techniques used fail to achieve the same results as are seen for lower resolution BSE micrographs (Figure 3). The trainable Weka segmentation algorithm goes a long way towards solving the issue, but is slow, memory intensive and struggles to identify the different fractions with acceptable fidelity. It is possible that other machine learning systems for either segmentation or background correction could achieve better results. Unfortunately, segmentation of SE-micrographs was ultimately unsuccessful using the described approaches (Figure 5).

Increased resolution was achieved by transition to SE, and the resulting images can be examined qualitatively. Reconstruction of a 3D volume is, however, impractical given the reduced material contrast.

Observed phenomena

As volumes were recorded, examples of GCC particles embedded within cellulose capsules (Figure 3) became evident for samples with added CNF. We note

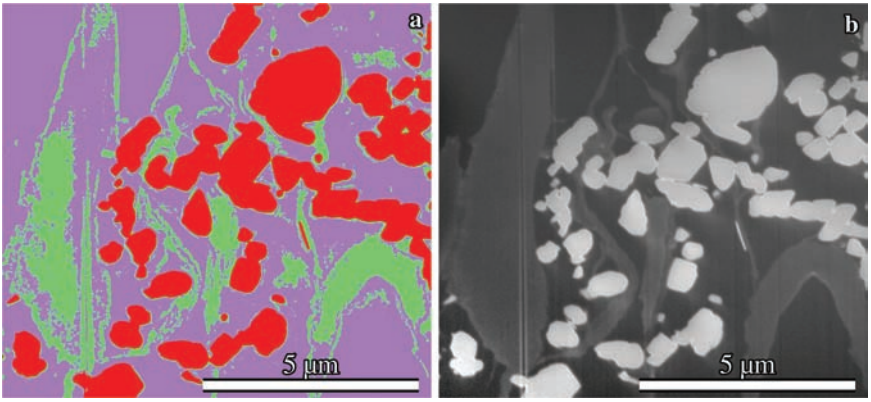

Figure 5. Trainable Weka Segmentation result (a) and the original (levelled) SE micrograph (b). In the segmented image (a), epoxy is colored purple, cellulose is green and GCC is red. GCC is identified with comparably low error margin. Cellulose and epoxy are not clearly recognized as separate phases due to variations in pixel brightness. In the levelled micrograph (b) GCC is brightest, cellulose is intermediate and the epoxy is darkest.

that these capsules are largely separated from the GCC particles by a void of varying size. Such voids, which in the recorded volumes are seen to frequently reach distances close to or well within the wavelengths of visible light (400–700 nm), will contribute to paper opacity.

We believe this phenomenon, as illustrated in Figure 6, occurs during the drying process. Associations between CNF and GCC in the imaged samples may have occurred, at least in part, due to the retention aids used in handsheet formation [10]. To the extent that this is the causative factor, any chemical association will likely be primarily electrostatic in nature, due to the retention aids used. As the CNF dries, swelling will inevitably decrease. As water is removed from the CNF the material can contract, forming bonds between fibrils and to other, chemically compatible components in the surrounding matrix, such as cellulose fibers. If this CNF encases a hypothetical, spherical GCC particle (hereafter called cargo), we can expect the external diameter of the gelated coating to shrink, while the internal diameter will attempt to increase. Should the forces between CNFs exceed the forces between CNF and cargo, the capsule-cargo bonds will be broken. While contact may be retained on portions of the cargo particle surface (Figure 6), a separate, independent capsule enclosing the cargo will form.

Figure 7 shows the same phenomenon in two different settings. Figure 7 a shows a CNF film containing 10 wt% GCC. While the film was not examined using FIB/SEM the cross-section reveals the introduction of faults around GCC particles or clusters of these. Both the film and the coated base board (Figure 7)

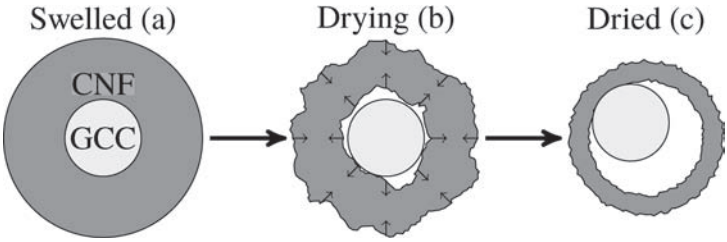

Figure 6. CNF encasing a spherical GCC particle when gelated, releasing it during drying, retaining contact on only a portion of the associated particle.

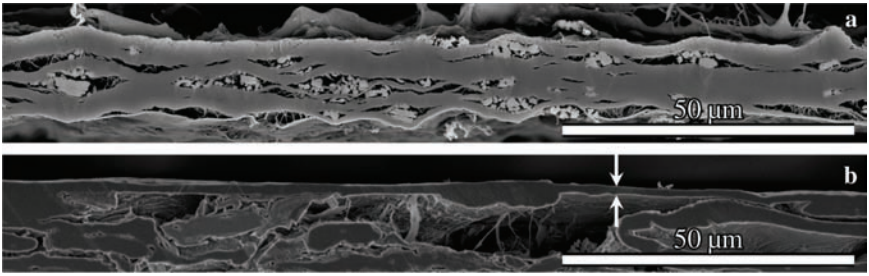

Figure 7. (a) is a backscatter electron micrograph showing a crossection of a CNF film with 10 wt% added GCC. A large number of cavities enclosing filler particles are seen across the imaged sample. (b) is reproduced from Ottesen *et al.* [9]. (b) shows a CNF coating applied to a rough liner board, separated from the substrate forming an independent film suspended across the base board surface pores. Arrows point to coating film. Contrast has been adjusted.

reveal that the phenomenon can also be seen on larger scales than what has been revealed by high resolution FIB/SEM examination discussed in the current work.

From the observed complexes, we can see that the voids between the capsule wall and the cargo frequently are sufficiently thick to represent a scattering event for incident light. Such interfaces will be beneficial to preserving opacity in paper, which commonly decreases when CNF is added [24]. It is furthermore possible this effect is the underlying mechanism for the observed properties reported for premixing of CNF and GCC [10]; when CNF and filler materials are allowed to form such capsule/cargo complexes, the complex itself will readily form hydrogen bonds to the surrounding paper matrix. Such interactions are not something many filler materials like GCC or clay allow without modification of their surface chemistry. The trapping of filler particles in capsules with only intermittent

physical contact between capsule and cargo could potentially aid in both retention of filler particles and preservation of paper opacity.

The observed capsules appear largely uneven in thickness, and discontinuities are seen on the observed complexes. This may in part be a result of the heterogeneity of the mechanically produced CNF fibrils. Were finer, more homogenous fibrils to be used, it is conceivable the capsule uniformity would increase and discontinuities decrease. This would be congruent with results reported for coatings applied from such qualities [9].

In paper and board, such complexes may act as contributors to light scattering and, potentially, filler retention. Furthermore, the presence of such complexes in paper may suggest that construction of whole, hollow capsules completely encasing cargo particles might be possible, independent of a surrounding paper matrix. Potential uses for such complexes may prove to be of interest outside conventional paper production. Such complexes could make use of the hygroscopic nature of cellulose to control the permeability of the capsule. By tuning the relative humidity in the capsule's surroundings, its permeability may be controlled. Possible uses for such systems could include controlled release of small quantities of volatile, gaseous contents, or controlled exposure of an enclosed sensor molecule to surrounding gases or hydrophobic liquids. It is made increasingly useful by the transparency of highly fibrillated CNF qualities, permitting the use of optical techniques to observe the enclosed sensors or study events within the capsules.

CONCLUSION

Using FIB/SEM, sufficient resolution to observe CNF in three dimensions within a paper matrix can be achieved. While imaged volumes are limited, features a few nm large can be resolved. This enables researchers to explore CNF interactions and distribution within the paper structure using a truly nanoscopic resolution in three dimensions, previously unmatched for paper characterization.

Both SE and BSE are shown to be possible signal sources for this investigation, achieving a resolution in the plane down to approximately 7 × 9 nm using SE. Resolutions this high were achieved using SE, at the cost of reliable contrast, making segmentation and quantitative analysis difficult.

Recorded volumes show instances of CNF encapsulating GCC when used together in handsheets. These capsules were observed to enclose, yet be largely independent of the GCC particles or clusters. This phenomenon is believed to occur during drying of CNF when a sufficient amount of it encases an object such as a GCC particle.

Our results demonstrate that FIB/SEM tomography has potential as a method for the study of nanocellulose interactions in paper and, conceivably, other

materials. The technique provides currently unparalleled 3D resolution and can provide a basis for improved understanding of CNF's behavior within a material to which it is added, e.g. in a paper matrix.

ACKNOWLEDGEMENTS

This work is performed as a part of the NORCEL Project: The NORwegian NanoCELlulose Technology Platform, initiated and led by The Paper and Fiber Research Institute (PFI) in Trondheim and funded by the Research Council of Norway through the NANO2021 Program (grant 228147 Research Council of Norway). The Research Council of Norway is further acknowledged for the support to the Norwegian Micro- and Nano-Fabrication Facility, NorFab. Special thanks go to Vinay Kumar and Martti Toivakka from Åbo Akademi for collaboration on related work [9]. Thanks are also extended to Gary Chinga-Carrasco (PFI) for fruitful conversations on image processing, Per Olav Johnssen (PFI) for collaboration and assistance on sample preparation techniques, and Kelly McCammon-Ottesen for proof-reading.

REFERENCES

1. N. Lavoine, I. Desloges, A. Dufresne and J. Bras. Microfibrillated cellulose – Its barrier properties and applications in cellulosic materials: a review. *Carbohydr. Polym.* **90**(2): 735–64, 2012.
2. S. H. Osong, S. Norgren and P. Engstrand. Processing of wood-based microfibrillated cellulose and nanofibrillated cellulose, and applications relating to papermaking: A review. *Cellulose* **23**(1): 93–123, 2016.
3. T. Lindstrom, A.Naderi and A. Wiberg. Large scale applications of nanocellulosic materials – A comprehensive review. *J. Korea Tech. Assoc. Pulp Pap. Ind.* **47**(6): 5–21, 2015.
4. F. W. Brodin, Ø. W. Gregersen and K. Syverud. Cellulose nanofibrils: Challenges and possibilities as a paper additive or coating material – A review. *Nord. Pulp Pap. Res. J.* **29**(1): 156–166, 2014.
5. S. Paunonen. Strength and barrier enhancements of composites and packaging boards by nanocelluloses – A literature review. *Nord. Pulp Pap. Res. J.* **28**(2): 165–181, 2013.
6. D. Klemm, F. Kramer, S. Moritz, T. Lindström, M. Ankerfors, D. Gray and A. Dorris. Nanocelluloses: A new family of nature-based materials. *Angew. Chem. Int. Ed. Engl.* **50**(24): 5438–66, 2011.
7. P. J. Heard, J. S. Preston, D. J. Parsons, J. Cox and G. C. Allen. Visualisation of the distribution of ink components in printed coated paper using focused ion beam techniques. *Colloids Surfaces A Physicochem. Eng. Asp.* **244**(1–3): 67–71, 2004.

8. K. Narayan and S. Subramaniam. Focused ion beams in biology. *Nat. Methods* **12**(11): 1021–1031, 2015.
9. V. Ottesen, V. Kumar, M. Toivakka, G. Chinga-Carrasco, K. Syverud and Ø.W. Gregersen. Viability and properties of roll-to-roll coating of cellulose nanofibrils on recycled paperboard. *Nord. Pulp Pap. Res. J.* **32**(2): In press, 2017.
10. V. Ottesen, K. Syverud and Ø.W. Gregersen. Mixing of cellulose nanofibrils and individual furnish components: Effects on paper properties and structure. *Nord. Pulp Pap. Res. J.* **31**(3): 441, 2016.
11. Fiji: an open-source platform for biological-image analysis. *Nat. Methods* **9**(7): 676–82, 2012.
12. D. Lowe. Object recognition from local scale-invariant features. In *Proc. Seventh IEEE Int. Conf. Comput. Vis.* IEEE, 1150–1157 vol. 2.
13. S. R. Sternberg. Biomedical image processing. *Computer (Long. Beach. Calif)*. **16**(1): 22–34, 1983.
14. R Core Team. *R: A Language and Environment for Statistical Computing* [Computer software] vol. 0: 2015.
15. C. Quammen. *Nonuniform Background Removal* [Computer software], 2007.
16. N. Bonnet. *A Posteriori Shading Correction* [Computer software], 2005.
17. I. Arganda-Carreras, V. Kaynig, C. Rueden, K. W. Eliceiri, J. Schindelin, A. Cardona and H. S. Seung. Trainable Weka Segmentation: a machine learning tool for microscopy pixel classification. *Bioinformatics*, 1–3, 2017.
18. J. Liu. High-resolution and low-voltage FE-SEM imaging and microanalysis in materials characterization. *Mater. Charact*. **44**(4): 353–363, 2000.
19. D. C. Joy and C. S. Joy. Low voltage scanning electron microscopy. *Micron* **27**(3–4): 247–263, 1996.
20. *Image Formation in Low-voltage Scanning Electron Microscopy*. SPIE Optical Engineering Press: Bellingham, 1993.
21. *Low Voltage Electron Microscopy: Principles and Applications* (ed. D. C. Bell and N. Erdman). John Wiley & Sons, Ltd: Chichester, 2012.
22. *Focused Ion Beam Systems: Basics and Applications* (ed. N. Yao). Cambridge University Press: Cambridge, 2007.
23. F. Santoro, E. Neumann, G. Panaitov and A. Offenhäusser. FIB section of cell-electrode interface: An approach for reducing curtaining effects. *Microelectron. Eng.* **124**: 17–21, 2014.
24. Ø. Eriksen, K. Syverud and Ø. Gregersen. The use of microfibrillated cellulose produced from kraft pulp as strength enhancer in TMP paper. *Nord. Pulp Pap. Res. J.* **23**(3): 299–304, 2008.

Transcription of Discussion

FOCUSED ION BEAM TOMOGRAPHY AS A MEANS FOR CHARACTERIZATION OF CNF IN A PAPER MATRIX

Vegar Ottensen,[1] *Erik Dobloug Roede,*[1]
Kristin Syverud[1,2] *and Øyvind Weiby Gregersen*[1]

[1] Norwegian University of Science and Technology (NTNU), Department of Chemical Engineering, Høgskoleringen 1, 7491 Trondheim, Norway
[2] Paper and Fibre Research Institute (PFI), Høgskoleringen

Ron Peerlings Eindhoven University of Technology

You showed that the two detectors BSE and SE give you complementary information, and it looks as if you do the segmentation on one at a time, either on BSE or SE. But wouldn't you be able to combine that information and then do the segmentation taking into account both sets of images?

Vegar Ottesen Norwegian University of Science and Technology

I wish, but it was not possible with our instruments. You could either image with secondary or backscatter. If you have a better FIB/SEM, then I will be happy to use it.

Ron Peerlings

Related to that, are you taking into account the depth direction in the segmentation? So in one image you of course know the image below and above, and you might take that information into account as well to get a better segmentation.

Discussion

Vegar Ottesen

Yes, we are taking that into account.

Jean-Claude Roux Grenoble Institute of Technology

You have mentioned that GCC was encased in the cellulose. Did you see this on the macroscopic scale?

Vegar Ottesen

No, we have not. We are in the process of replicating it on the macroscopic scale. Beyond what we showed here, we have not replicated on the macroscopic scale now.

Vikram Singh Raghuwanshi Monash University

I would just like to know how much depth you can penetrate with the beam to get the information about internal structure?

Vegar Ottesen

We have recorded volumes of about 10×10×10 micrometres, but there is no real upper limit, if you zoom out a little bit and reduce your resolution, you can go significantly larger.

Vikram Singh Raghuwanshi

And the second question, you only use cellulose, is there any other kind of biological material you can use for these kinds of studies?

Vegar Ottesen

This particular instrument and the technique has been used at our university to study the subcellular features in, for example, cancer cells.

Warren Batchelor Monash University

Could you potentially just dye a few of your cellulose nanofibres and use that to look at what happens to the nanofibres in your structure?

Vegar Ottesen

Yes, we could. We have not done so now. We stained the sample after we created the handsheet, but there is, in principal, no reason you couldn't stain the fibrils beforehand.

Tero Tuovinen University of Jyväskyjlä

I noticed that in the video that you showed about the secondary vertical imaging, there were just vertical lines at the left. It looks like some sort of artifact, but do you know what process causes that?

Vegar Ottesen

Yes, it's interactions with the ion beam. We were more careful with the ion beam parameters for this image than we were when we tried to demonstrate the artifacts. However, local variations in the structure may have caused their origin despite more care taken with the ion beam parameters.

Toshiharu Enomae University of Tsukuba, Japan

My question is about the drying process of the CNF encasing the GCC particle. In the third (stage C), of Figure 3, it shows the cavity in dried CNF is getting larger than that in the drying stage B. The CNF wall shrinks inward, but the inner cavity is getting bigger. Is this possible?

Vegar Ottesen

We would guess that the fibrils on the inner side would contract out towards the mid-point of the ring, while the outer fibrils contract inwards. That's what we surmise. The same thing that would happen if you shrink a gel in another situation, it shrinks in both directions not just out and in.

Toshiharu Enomae

Yes, it would be very good to prove what is happening during the drying stage.

Vegar Ottesen

This is just a hypothesis so far, we are in the process of testing it.

Doug Coffin Miami University, Oxford, OH

Now you have a resolution of 7×9×50 nm. Is that resolution enough to gain insights into the actual structure of the nano cellulose fibrils, or what kind of form they take when put into these structures?

Vegar Ottesen

It should be. The images that I showed you for the secondary electron, this volume that I chose here is from a controlled sample without nanocellulose, but we have recorded some that do contain it, and the resolution is certainly sufficient to see all but the smaller fibrils. So, you should be able to gain some insight if you apply this to more samples.

Doug Coffin

So, you have not done that yet?

Vegar Ottesen

We have done the measurements here which describe some of the interactions such as the capsule formation. Beyond that, we haven't made any.